Precipitation-Top Heights of Heavy Orographic Rainfall in the Asian Monsoon Region

SHOICHI SHIGE

Graduate School of Science, Kyoto University, Kyoto, Japan

CHRISTIAN D. KUMMEROW

Department of Atmospheric Science, Colorado State University, Fort Collins, Colorado

(Manuscript received 8 September 2015, in final form 28 April 2016)

ABSTRACT

Over coastal mountain ranges of the Asian monsoon region, heavy orographic rainfall is frequently associated with low precipitation-top heights (PTHs). This leads to conspicuous underestimation of rainfall using microwave radiometer algorithms, which conventionally assume that heavy rainfall is associated with high PTHs. Although topographically forced upward motion is important for rainfall occurrence, it does not fully constrain precipitation profiles in this region. This paper focuses on the thermodynamic characteristics of the atmosphere that determine PTHs in tropical coastal mountains of Asia (Western Ghats, Arakan Yoma, Bilauktaung, Cardamom, Annam Range, and the Philippines).

PTHs of heavy orographic rainfall generally decrease with enhanced low- and midlevel relative humidity, especially during the summer monsoon. In contrast, PTHs over the Annam Range of the Indochina Peninsula increase with enhanced low-level and midlevel relative humidity during the transition from boreal summer to winter monsoon, demonstrating that convection depth is not simply a function of humidity. Instead, PTHs of heavy orographic rainfall decreased with increasing low-level stability for all monsoon regions considered in this study, as well as the Annam Range during the transition from boreal summer to winter monsoon. Therefore, low-level static stability, which inhibits cloud growth and promotes cloud detrainment, appears to be the most important parameter in determining PTHs of heavy rainfall in the Asian monsoon region.

1. Introduction

The prevailing view that heavy rainfall results from cumulonimbus with a considerable vertical extent of radar echo is generally attributed to observational studies in the United States, such as the pioneering work of Byers and Braham (1949). Cumulonimbus clouds also exhibit lightning and thunder related to strong cold-rain processes, leading to their common designation as thunderstorms (Cotton et al. 2011; Houze 2014). Under this paradigm, some studies use "deep convection" as synonymous with "heavy precipitation." For example, Xie et al. (2006) wrote about the important role of narrow mountains in the Asian monsoon region, but noted, "In the Asian monsoon region, by contrast, orographic induced deep convection has large-scale effects because of its strong interaction with circulation" without examining the vertical structure of this convection.

However, Tropical Rainfall Measuring Mission (TRMM; Kummerow et al. 1998) measurements demonstrate that heavy rainfall is not necessarily associated with conventional high echo-top heights but, rather, with relatively low echo-top heights. Sohn et al. (2013) showed that the majority of summer rainfall over the Korean peninsula is "warm type," with TRMM Precipitation Radar (PR) echo-top heights lower than 8 km. Furthermore, clouds over Korea are not as high as the deep convective clouds found in Oklahoma in the United States, even though surface rain rates are equal. Recently, Hamada et al. (2015) showed that most extreme rainfall events in the tropics and subtropics are characterized by less intense convection, with intense radar echoes that do not extend to extremely high altitudes.

Corresponding author address: Shoichi Shige, Graduate School of Science, Kyoto University, Kiashirakawa-Oiwake-cho, Sakyo-ku, Kyoto 606-8502, Japan.
E-mail: shige@kugi.kyoto-u.ac.jp

DOI: 10.1175/JAS-D-15-0271.1

Many satellite rainfall algorithms have been developed under the paradigm that heavy rainfall is associated with high echo-top heights. Infrared radiometer algorithms relate the rainfall rate to the cloud brightness temperature, implicitly assuming that deeper, colder clouds are more likely to produce heavy rainfall (e.g., Richards and Arkin 1981). More recently, microwave radiometers (MWRs) have become the principal sensors for global precipitation retrievals. Over ocean, MWRs provide a more direct relationship to rain rates using emission signatures from liquid water over a spectrum of lower-frequency channels (Ebert and Manton 1998). Over land, however, MWR algorithms relate the rainfall rate to scattering signatures from ice crystals over a spectrum of higher-frequency channels, implicitly assuming that deeper clouds with more precipitation-sized ice are more likely to produce heavy rainfall (e.g., Spencer 1984; McCollum and Ferraro 2003; Weng et al. 2003; Ferraro et al. 2005).

Conspicuous underestimation of rainfall by MWR algorithms, such as the Goddard profiling (GPROF) algorithm (Kummerow et al. 2015) and the Global Satellite Mapping Precipitation (GSMaP) MWR algorithm (Aonashi et al. 2009; Shige et al. 2009a), occurs in coastal mountains of the Asian monsoon region, including Japan (Kubota et al. 2009), Korea (Kwon et al. 2008), Taiwan (Taniguchi et al. 2013), and India (Shige et al. 2015, hereafter S15). In these areas, heavy rainfall is frequently associated with low precipitation-top heights (PTHs), which is inconsistent with the conventional assumption that heavy rainfall is associated with high PTHs. PTHs for convective precipitation profiles with surface rain rates of 10–50 mm h^{-1} are located at heights from 0.5 to 1.5 km and from 2.0 to 4.0 km above the freezing level for the Kii Peninsula and the west coast of India, as shown in Fig. 2.7c of S15 and Fig. 2.7e of S15, where PTH is defined by thresholds of 0.5 mm h^{-1}. They are distinctly lower than PTHs for conventional precipitation profiles over land shown in Fig. 2.7a of S15, which are 4.0–6.0 km above the freezing level. This type of heavy orographic rainfall is thought to be consistent with the warm-type rainfall described in Sohn et al. (2013), as well as ''medium-depth convection'' described in Zhang et al. (2006).

An orographic–nonorographic rainfall classification scheme to identify orographic rainfall with low PTHs has been incorporated into the GSMaP MWR algorithm (Shige et al. 2013; S15; Taniguchi et al. 2013; Yamamoto and Shige 2015). This classification scheme is based on topographically forced upward motion and convergence of surface moisture flux. Yamamoto and Shige (2015) showed that this scheme improves rainfall estimation over the entire Asian region. However, they showed low verification scores over the Sierra Madre of Mexico, because of its tall precipitation profiles (even for orographic rainfall conditions). This implies that topographically forced upward motion and convergence of surface moisture flux do not fully constrain precipitation profiles in this area.

Issues identified in the MWR rainfall algorithms are related to fundamental questions about what thermodynamic parameters determine PTHs. In this study, we examine the relationship between various thermodynamic characteristics of the atmosphere and the PTH of relatively heavy orographic rainfall in tropical coastal mountains, with an emphasis on the Asian monsoon region. Coastal mountains in the tropics are good natural laboratories in which to explore PTHs, because of their simple forcing mechanism of convection but also their seasonally and spatially variable precipitation profiles in coastal areas (Petersen and Rutledge 2001). As reviewed by Roe (2005), Lin (2007), and Houze (2012), mountains and hills affect precipitating clouds via several mechanisms; however, in this study, only rainfall enhanced by the topographically forced vertical motion on windward slopes is considered.

2. Data and methods

We used TRMM PR 2A25, version 7 (V7), data (Iguchi et al. 2009) over a 5-yr period (2004–08) on a 0.05° grid. The European Centre for Medium-Range Weather Forecasts (ECMWF) interim reanalysis (ERA-Interim; Dee et al. 2011) was used to describe the atmospheric environment, having a resolution of 0.75° × 0.75° at 6-hourly intervals.

The nine boxes (2.25° × 2.25°) of ERA-Interim, in which the center box includes a PR raining grid, are defined as a target region (Fig. 1). We focused on the rain class with $10 < R \leq 40$ mm h^{-1}, where R is PR 2A25 V7 ''near-surface rain'' on a 0.05° grid. PTH increases with rainfall, even when heavy rainfall is associated with relatively low PTHs, as shown in Fig. 2 of Shige et al. (2013) and Fig. 2.7 of S15; thus, we set an upper limit. The numbers of grids with $10 < R \leq 40$ mm h^{-1} were 136 020 for the Western Ghats, 68 472 for Arakan Yoma, 38 896 for Bilauktaung, 24 064 for Cardamom, 83 992 for the Annam Range, 21 012 for the Philippines, and 73 080 for Mexico. Cases having $R > 40$ mm h^{-1} will be discussed later.

In this study, the atmosphere is separated into low and midlevels at 4.5-km height; this is close to the climatological 0°C level. A low-level upstream region among the eight boxes surrounding the 2.25° × 2.25° boxes is determined using the average wind direction below 4.5-km height over the target region $\mathbf{V}_{\mathrm{low}}$. A midlevel upstream

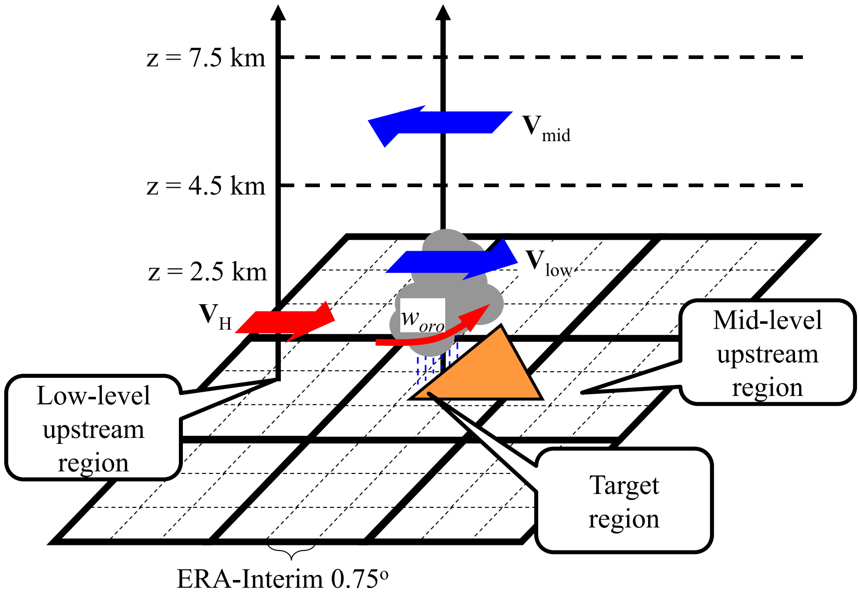

FIG. 1. Schematic of the target region with low- and midlevel upstream regions.

region is determined using the average wind direction between 4.5- and 7.5-km heights over the target region $\mathbf{V}_{\mathrm{mid}}$. Orographically forced vertical motion may be roughly estimated from the lower boundary condition for flow over mountains (Lin 2007):

$$w_{\mathrm{oro}} = \frac{Dh(x,y)}{Dt} = \mathbf{V}_{\mathrm{H}} \cdot \nabla h(x,y), \qquad (1)$$

where $h(x, y)$ is the elevation (m) derived from the Shuttle Radar Topography Mission (SRTM30; Werner 2001; Farr et al. 2007), with horizontal grid spacing of approximately 1 km, averaged over a 50-km horizontal length scale for the calculation of w_{oro}, after Taniguchi et al. (2013). In Eq. (1), $\mathbf{V}_{\mathrm{H}}$ is the average horizontal wind (m s^{-1}) below 2.5 km over the upstream region. This is used because low-level jets with a wind speed maximum in the lowest few kilometers of the atmosphere occur even though surface winds are weak (Stensrud 1996), and only low-scale mountain ranges (~1 km in height) are considered in this study. The appropriate height range for $\mathbf{V}_{\mathrm{H}}$ varies with the height of the mountains, but using surface winds for $\mathbf{V}_{\mathrm{H}}$ does not markedly change these results.

Here, we investigate six thermodynamic parameters (Table 1) over the upstream region that are candidates for determining PTH for rainfall enhanced by the orographically forced upward motion on windward slopes ($w_{\mathrm{oro}} > 0$ m s^{-1}). The first parameter is potential instability, also known as convective instability, which describes an atmospheric state where the atmospheric layer becomes statically unstable after lifting. Here, potential instability is defined as the gradient of equivalent potential temperature ($d\theta e/dz$) in the lower troposphere (1.5 and 4.5 km). The second parameter is static stability near the 0°C level, which previous studies (e.g., Johnson et al. 1999) considered to contribute to the formation of cumulus congestus over tropical oceans by inhibiting cloud growth and promoting cloud detrainment. To form a measure of static stability near the 0°C level, we calculate

$$dT_v/dz_{\mathrm{mlt}} = \frac{T_v(z_{k+1}) - T_v(z_k)}{z_{k+1} - z_k} \quad \text{if} \quad T_v(z_{k+1}) < 0 \quad \text{and} \quad T_v(z_k) \geq 0, \qquad (2)$$

where T_v is the virtual temperature (°C). The third and fourth parameters are relative humidity of the lower troposphere ($\mathrm{RH}_{\mathrm{low}}$) and midtroposphere ($\mathrm{RH}_{\mathrm{mid}}$). The fifth and sixth parameters are static stability from

TABLE 1. Thermodynamic parameters used in this study.

Parameter	Description
$d\theta_e/dz$	Potential instability from 1.5 to 4.5 km
dT_v/dz_{mlt}	Static stability near the 0°C level
$\mathrm{RH}_{\mathrm{low}}$	Relative humidity of the lower troposphere from 1.5 to 4.5 km
$\mathrm{RH}_{\mathrm{mid}}$	Relative humidity of the midtroposphere from 4.5 to 7.5 km
dT_v/dz_{low}	Static stability of the lower troposphere from 1.5 to 4.5 km
dT_v/dz_{mid}	Static stability of the midtroposphere from 4.5 to 7.5 km

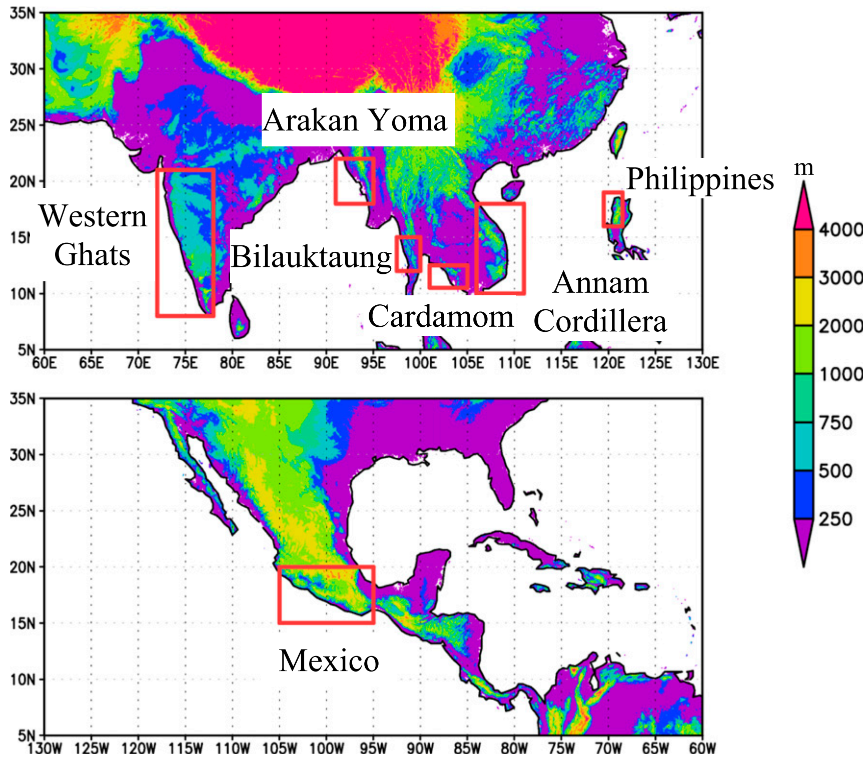

FIG. 2. Location of mesoscale mountain ranges of (top) the South Asian monsoon region (Western Ghats, Arakan Yoma, Bilauktaung, Cardamom, Annam Range, and the Philippines) and (bottom) Mexico.

$z = 1.5$ to 4.5 km (dT_v/dz_{low}) and from $z = 4.5$ to 7.5 km (dT_v/dz_{mid}).

3. Overview of the Asian monsoon region

We investigated heavy rainfall over six mesoscale coastal mountain ranges (Western Ghats, Arakan Yoma, Bilauktaung, Cardamom, Annam Range, and the Philippines) within the South Asian monsoon region (Fig. 2, top), following sites selected in Xie et al. (2006). Average elevations are ~1 km, except for the Philippines (~1.5 km). We also examined heavy rainfall over Mexico (~2.0–2.5 km) for comparison (Fig. 2, bottom). In this area, strong cold-rain processes dominate and the orographic–nonorographic rainfall classification scheme was switched off in the GSMaP MWR algorithm.

Of these six mountain ranges, only the Philippines belongs to the western North Pacific summer monsoon region, where continental influences are less significant; the others belong to the Southeast Asian summer monsoon region (Murakami and Matsumoto 1994). Wang and LinHo (2002) separated these five ranges into the Indian summer monsoon region (Western Ghats and Arakan Yoma) and the Indochina Peninsula (Bilauktaung, Cardamom, and Annam Range), which comprises a broad "buffer" zone between the Indian summer monsoon region and western North Pacific summer monsoon region.

The annual cycle of rainfall in the Annam Range and the Philippines differs from that of the other mountain ranges because of wind–terrain interactions (Chang et al. 2005). A wind reversal takes place over the South China Sea and the western Pacific in October, causing onshore northeasterly monsoon winds toward the eastern flank of the Annam Range and the Philippines, contributing to significant rainfall (Xie et al. 2006). Thus, the Annam Range is directly affected by onshore northeasterly monsoon winds. The eastern flank of the Philippines is excluded from this study (Fig. 2) to confine our analysis to a single meteorological regime.

Longitude–height cross sections of the 5-yr unconditional mean heating ($Q_1 - Q_R$) profiles along latitude line 18°N for the summer [June–September (JJAS)] season are plotted in Fig. 3. These profiles are compiled from the spectral latent heating product (TRMM PR 3H25; Shige et al. 2004, 2007, 2008, 2009b), where Q_1 is the apparent heat source (Yanai et al. 1973) and Q_R is the radiative heating, with horizontal winds

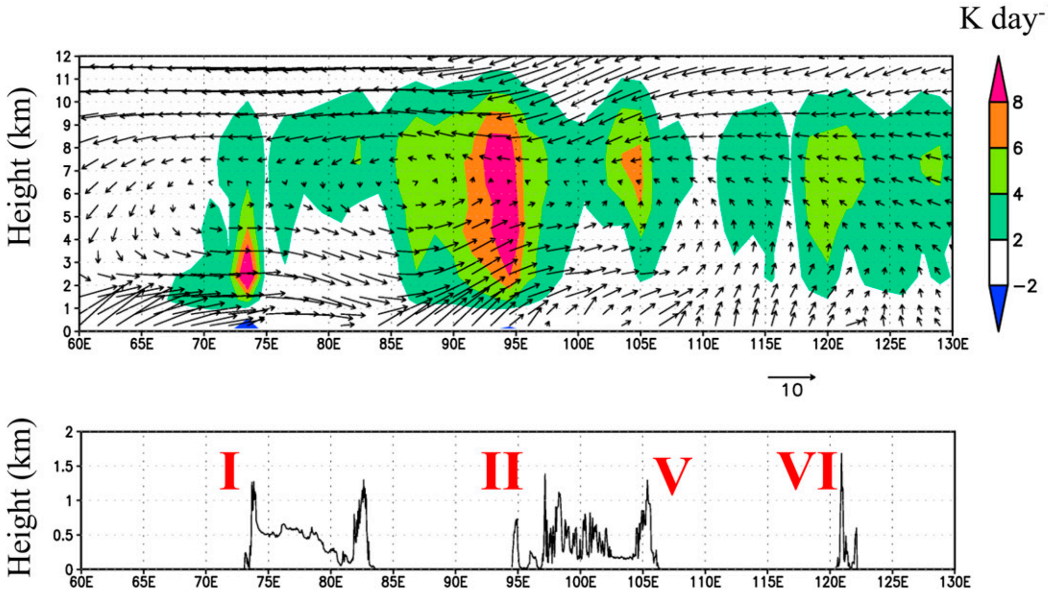

FIG. 3. (top) Longitude–height cross sections of the 5-yr unconditional mean heating ($Q_1 - Q_R$) along 18°N for JJAS estimated using the spectral latent heating algorithm from TRMM PR data and horizontal wind, along with (bottom) topography. Mountain ranges shown in this figure are Western Ghats (I), Arakan Yoma (II), Annam Range (V), and the Philippines (VI).

from ERA-Interim and topography from SRTM30. Over the summer monsoon, southwesterly flow impinges on the western side of these coastal mountain ranges and strong heating takes place associated with narrow rainbands on their western sides, which correspond to their coastal sides, except for the Annam Range.

The horizontal variation of the vertical distribution of heating can be seen in Fig. 3. In particular, strong low-level heating is found over the Western Ghats. Using the convective stratiform heating product (Tao et al. 2010), Kumar et al. (2014) showed that shallower clouds appear more frequently over the Western Ghats, while there are deeper clouds over the Myanmar coast. Xie et al. (2006) demonstrated that imposed narrow bands of diabatic heating with a peak at 500–300 hPa on the west coast of Myanmar and the Philippines, as well as on the slope of the Annam Range, exert far-reaching effects on the continental-scale monsoon, leading to considerable improvements in the simulations of the large-scale monsoon. The effects of shallow heating occurring on the west slope of the Western Ghats on the large-scale circulation is interesting but beyond the scope of this study. Heating over the Arakan Yoma appears to be part of the broader heating occurring over the Bay of Bengal, implying that rainfall over the Bay of Bengal is produced not only by in situ orographically driven convection but also by northward-propagating convection of monsoon intraseasonal oscillations (Hoyos and Webster 2007).

4. Relationships between precipitation-top heights and thermodynamic parameters

Figure 4 shows precipitation profiles with near-surface rain rates of $10 < R \leq 40\,\mathrm{mm\,h^{-1}}$ as a function of w_{oro} for six coastal mountain ranges of the South Asian monsoon region, as well as Mexico. Here, PTH is defined by thresholds of $0.5\,\mathrm{mm\,h^{-1}}$, which correspond to 18.5 (stratiform) and 17.3 dBZ (convective) above the -15°C level. These values change slightly to account for dielectric properties of warmer hydrometeors, as defined by the PR 2A25, version 7, algorithm (Iguchi et al. 2009).

Strong negative correlation coefficients between w_{oro} and PTH were found over the Western Ghats (Fig. 4a), Cardamom (Fig. 4d), and Mexico (Fig. 4g), where PTHs reach well above the 0°C level for atmospheric downward motion, decreasing with orographically forced upward motion. However, relatively weak negative correlations were found over the Arakan Yoma (Fig. 4b) and the Annam Range (Fig. 4e), indicating that orographically forced upward motion may initiate convection, but it does not fully constrain precipitation profiles.

Comparisons of correlation coefficients between various thermodynamic quantities (Table 1) and PTHs for the six coastal mountain ranges of the South Asian

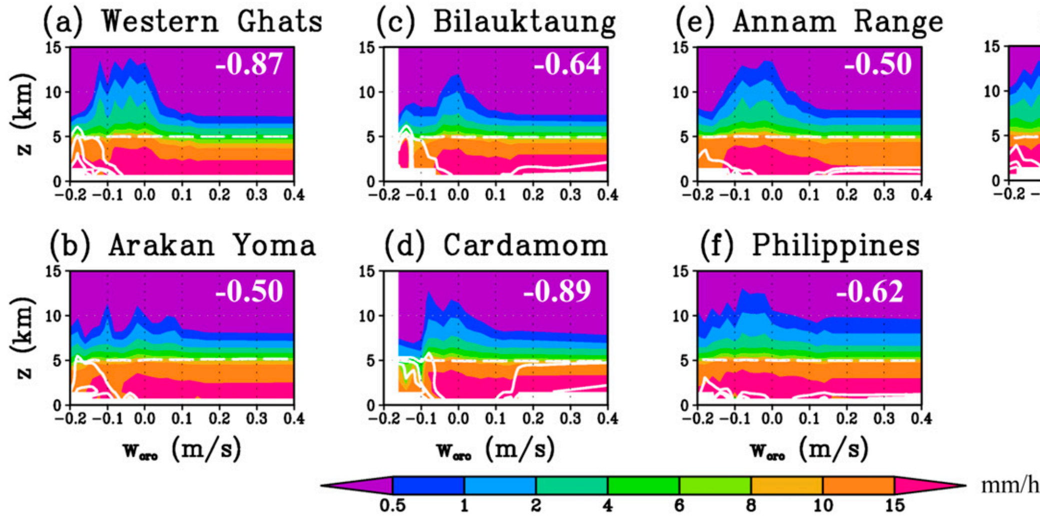

FIG. 4. Precipitation profiles with near-surface rain rates of $10 < R \leq 40\,\mathrm{mm\,h^{-1}}$ as a function of w_{oro}. The white dashed line indicates the 0°C level. White contours indicate values of the confidence interval for the mean at the 95% significance level of the Student's t test. The contour interval is $5\,\mathrm{mm\,h^{-1}}$. Correlation coefficients for precipitation-top heights with precipitation profiles having confidence intervals less than $5\,\mathrm{mm\,h^{-1}}$ above $z = 2.5$ km are indicated in the upper-right corner of each panel. Thresholds of $0.5\,\mathrm{mm\,h^{-1}}$ were used to detect precipitation-top height.

monsoon region and Mexico are summarized in Fig. 5. Correlation coefficients between dynamical quantities (i.e., w_{oro} and wind shear) and PTHs are also shown. Here, wind shear is defined as

$$\mathrm{WSHR} = \sqrt{(u_{\mathrm{mid}} - u_{\mathrm{low}})^2 + (v_{\mathrm{mid}} - v_{\mathrm{low}})^2}, \qquad (3)$$

where $\mathbf{V}_{\mathrm{low}} = (u_{\mathrm{low}}, v_{\mathrm{low}})$ and $\mathbf{V}_{\mathrm{mid}} = (u_{\mathrm{mid}}, v_{\mathrm{mid}})$. Note that PTHs are defined from precipitation profiles, with near-surface rain rates of $10 < R \leq 40\,\mathrm{mm\,h^{-1}}$ and upward motion ($w_{\mathrm{oro}} > 0\,\mathrm{m\,s^{-1}}$), to obtain correlation coefficients of thermodynamic parameters and wind shear with PTHs. Most of these thermodynamic parameters have consistently high correlation coefficients with PTHs in western parts of this region (Western Ghats, Arakan Yoma, Bilauktaung, and Cardamom) and Mexico. Relatively weak correlation coefficients (<0.6) for $d\theta_e/dz$, $\mathrm{RH_{low}}$, $\mathrm{RH_{mid}}$, and w_{oro} were found in Arakan Yoma, which may be attributed to the fact that rainfall over the Bay of Bengal is produced not only by the in situ and orographic driven convection but also by northward-propagating convection within monsoon intraseasonal oscillations (Hoyos and Webster 2007).

In the Annam Range and the Philippines, some of these parameters had low correlation coefficients with PTHs. In particular, wind shear had weak correlation coefficients in both ranges, possibly because of the wind reversal over the South China Sea and the western Pacific during the winter monsoon. This suggests that wind shear does not constrain precipitation profiles. Vertical wind shear could contribute to the maintenance of mesoscale convective systems as well as inhibit upright convection (Rotunno et al. 1988). Sherwood (1999) demonstrated that a linear model poorly represents the effects of wind shear on oceanic convection over the western Pacific; hence, convection may be aided by moderate shear values but inhibited by too much shear. The effects of wind shear on orographic rainfall are unquestionably important. As discussed in Houze (2012), the characteristics of the airflow over the terrain, combined with the terrain size and the microphysical time scales, determine whether precipitation particles will ultimately land on windward or leeward slopes of mountains. Given that only rainfall enhanced by orographically forced vertical motion on the windward

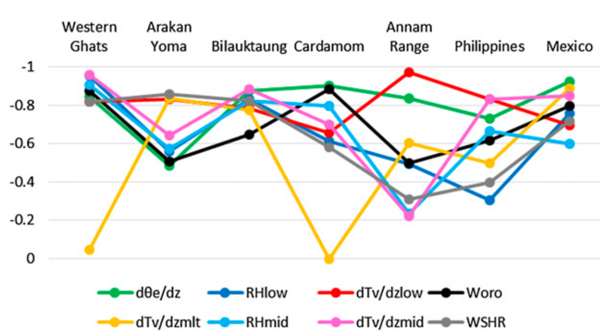

FIG. 5. Comparison of correlation coefficients of candidate thermodynamic and dynamical quantities with precipitation-top heights. Wind shear is abbreviated as WSHR.

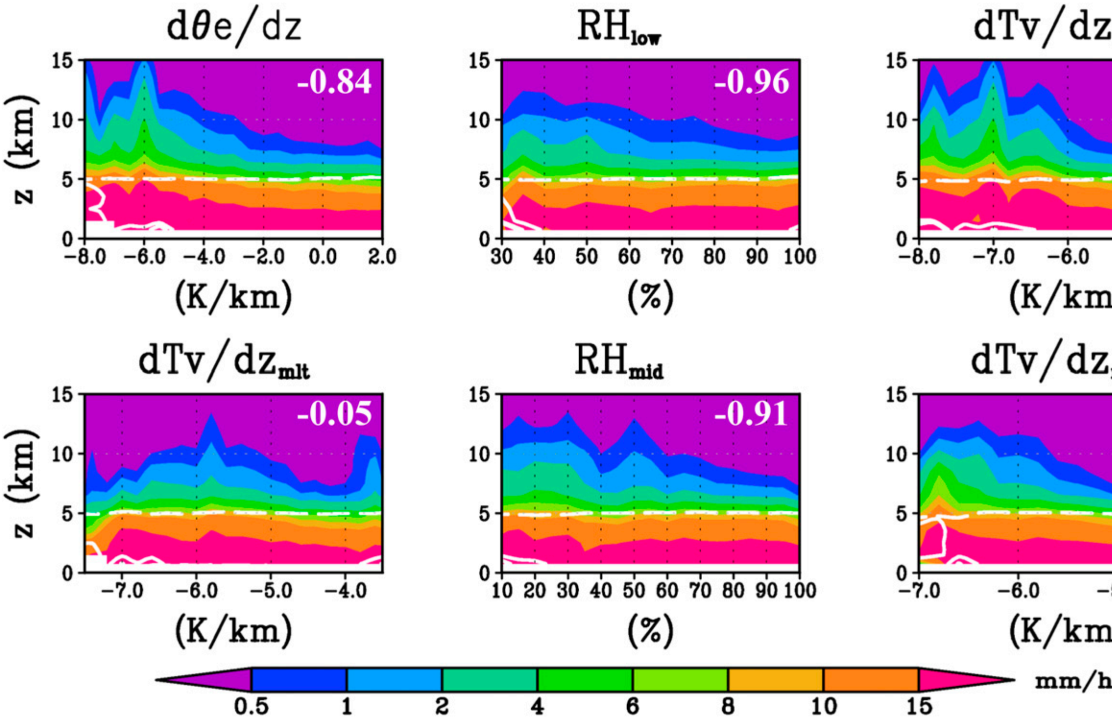

FIG. 6. As in Fig. 4, but for precipitation profiles with near-surface rain rates of $10 < R \leq 40\,\mathrm{mm\,h^{-1}}$ and orographically forced upward motion ($w_{\mathrm{oro}} > 0\,\mathrm{m\,s^{-1}}$) as a function of candidate thermodynamic parameters over the Western Ghats for all seasons during the study period 2004–08.

slopes is considered, this may contribute to a weak correlation. Although the effects of wind shear on orographic rainfall warrant further examination, we focus on the candidate thermodynamic quantities listed in Table 1. Wind shear is presented in Fig. 5 only to contrast its importance to the thermodynamic variables considered in this study.

5. Western Ghats and Annam Range

It is difficult to determine the key parameter controlling PTHs in the western areas of Asia (Western Ghats, Arakan Yoma, Bilauktaung, and Cardamom) and Mexico, where most of the thermodynamic parameters had consistently high correlation coefficients (Fig. 5). This suggests that they are closely related to each other, coupled under the influence of large-scale circulation. Hence, we examined results from the Annam Range in more detail, where there is a broad range of environmental conditions because of the onshore northeasterly monsoon winds from the South China Sea, as well as those in the Western Ghats, where orographic rainfall with low PTHs occurs frequently (Fig. 3).

Figure 6 shows precipitation profiles with near-surface rain rates of $10 < R \leq 40\,\mathrm{mm\,h^{-1}}$ and upward motion ($w_{\mathrm{oro}} > 0\,\mathrm{m\,s^{-1}}$) over the Western Ghats, as functions of the six candidate thermodynamic quantities. All parameters except for static stability near the 0°C level (dT_v/dz_{mlt}) had high correlation coefficients. Static stability near the 0°C level appears to have less influence on precipitation profiles than the other candidate thermodynamic quantities. Static stability near the 0°C level is likely related to the effects of melting (Johnson et al. 1996), which mainly occurs in deep stratiform ice clouds. Yasunaga et al. (2006) showed that the frequency peak of the stable layer near the 0°C level is more pronounced during the Madden–Julian oscillation active period with deep stratiform ice clouds, than during its inactive periods without deep stratiform ice clouds. As shown in Fig. 3, the heating profile showing strong low-level heating over the Western Ghats indicates a small contribution of deep stratiform ice clouds with upper-level heating and lower-level cooling. Occurrences of shallow convection without deep stratiform ice clouds yield low correlation coefficients for the Western Ghats, suggesting that there is no relationship between PTH and static stability near the 0°C level.

Our results for these areas are consistent with previous studies. Based on sensitivity tests with a cloud-resolving model, Takemi et al. (2004) showed that static

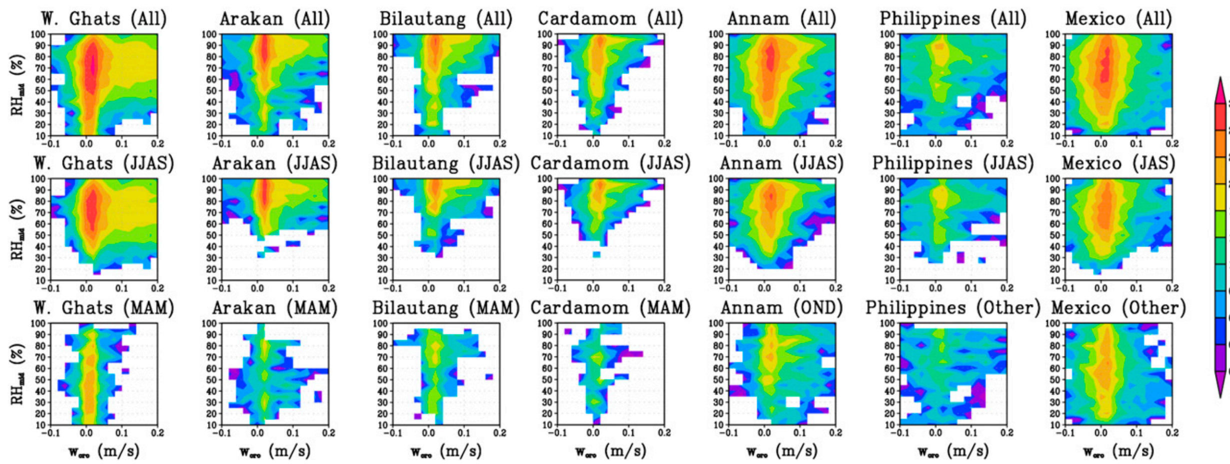

FIG. 7. Two-dimensional histogram of grids with heavy rain rates ($10 < R \leq 40\,\mathrm{mm\,h^{-1}}$) for the seven study regions as a function of w_{oro} and $\mathrm{RH_{mid}}$. Color contours indicate natural logarithms of the grid number.

stability near the 0°C level does not control the height of tropical oceanic convection. Using observations from an Atmosphere Radiation Measurement surface-based remote sensing site at Nauru Island, Jensen and DelGenio (2006) suggested that the 0°C stable layer is not effective at limiting oceanic congestus cloud-top heights. Takemi et al. (2004) and Jensen and DelGenio (2006), however, showed that a drying of the mid-troposphere is effective at limiting oceanic congestus cloud-top heights. Takayabu et al. (2006), based on sensitivity studies with a diagnostic cloud model, demonstrated that a low relative humidity at 600–800 hPa is a key factor limiting oceanic congestus cloud-top heights, which is coincident with conditions in the 0°C stable layer. Recently, Takayabu et al. (2010) argued that the entrainment of middle- to lower-tropospheric dry air, which accompanies large-scale subsidence, is the major factor suppressing deep convection. These studies suggest that PTHs increase with increasing relative humidity in the midtroposphere. However, the PTHs of heavy orographic rainfall decrease with increasing $\mathrm{RH_{low}}$ and $\mathrm{RH_{mid}}$ in the Western Ghats (Fig. 6). In Fig. 5, similar tendencies (i.e., high negative correlation coefficients with PTH) are found for the other ranges in Asia, except for the Annam Range and the Philippines, which have low negative correlation coefficients for $\mathrm{RH_{mid}}$ and $\mathrm{RH_{low}}$.

The above results are different from what is observed for convection over tropical oceans but are consistent with the fact that MWR algorithms, which assume that deeper clouds with precipitation-sized ice produce heavy rainfall, consistently underestimate precipitation during the summer monsoon (S15). Two-dimensional histograms of grids with heavy rain rates ($10 < R \leq 40\,\mathrm{mm\,h^{-1}}$) as function of w_{oro} and $\mathrm{RH_{mid}}$ are illustrated in Fig. 7 for the seven regions investigated in this study. Results for all seasons (Fig. 7, top) for the western part of the South Asian monsoon region (Western Ghats, Arakan Yoma, Bilauktaung, and Cardamom) show a clear horizontal and vertical feature, occurring at high $\mathrm{RH_{mid}}$ and $w_{oro} = 0.02\,\mathrm{m\,s^{-1}}$. The horizontal feature is best developed during the summer monsoon (JJAS) shown in the middle panels of Fig. 7, while the vertical feature is enhanced during the premonsoon [March–May (MAM)], as shown in the bottom panels of Fig. 7. Such features indicate how $\mathrm{RH_{mid}}$ changes in concert with the large-scale circulation. Heavy orographic rainfall in environments with high $\mathrm{RH_{mid}}$, where PTHs are low (Figs. 5 and 6), occurs during the summer monsoon. Similar results for $\mathrm{RH_{low}}$ were also obtained (not shown). These are consistent with the results of Manohar et al. (1999) that showed that the ratio of rainfall-to-thunderstorm days, as defined by Zipser (1994), is 3–4 times higher during the monsoon than during the premonsoon over the Indian region. This suggests there is a greater contribution from convection with low PTHs to rainfall during the monsoon than during the premonsoon. In East Asia, heavy orographic rainfall with low PTHs also is observed during the moist summer season (Takeda et al. 1976; Takeda and Takase 1980; Sakakibara 1981; Shige et al. 2013).

For the Annam Range (Fig. 7, bottom), October–December (OND) represents the transition from boreal summer to the winter monsoon (Yokoi and Matsumoto 2008). In the Philippines, there is a distinction between JJAS and the remaining or "other" months of the year. This is because the annual cycle of rainfall in both the Annam Range and the Philippines is affected by

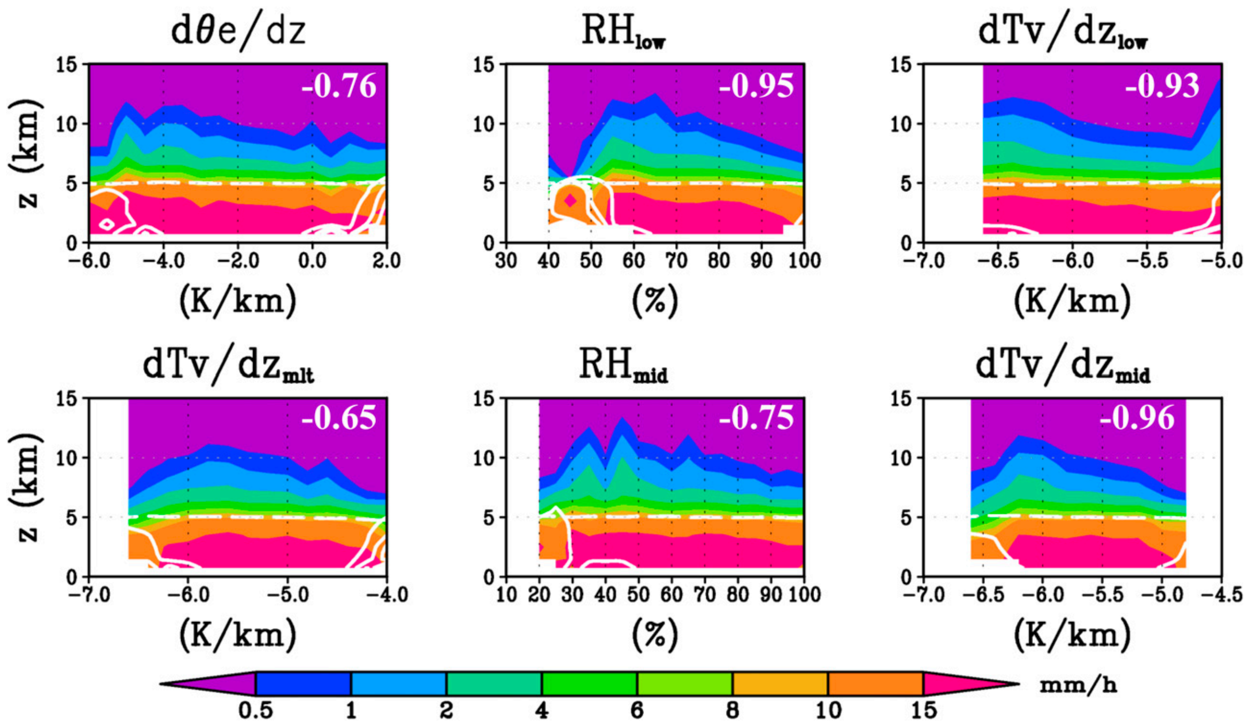

FIG. 8. As in Fig. 6, but for the Annam Range for the summer monsoon (June–September) during the study period 2004–08.

wind–terrain interactions (Chang et al. 2005), with little rain occurring during MAM. The middle panels in Fig. 7 show that the Annam Range and the Philippines are characterized by high RH_{mid} and a broad range in w_{oro} during JJAS, similar to other mountain ranges in this region. In contrast, heavy orographic rainfall over the Annam Range during OND, and over the Philippines over the remainder of the year, also occurs under low RH_{mid} with a broad range of w_{oro}, possibly leading to the low negative correlation coefficients observed in this study.

The Mexican monsoon (also called the North American monsoon; Douglas et al. 1993; Adams and Comrie 1997) is experienced as a pronounced increase in rainfall from an extremely dry June to a wet July, with rain falling until mid-September. Therefore, Mexican climate is separated into a rainy season [July–September (JAS)] and "other" months of the year. The results from Mexico do not show the same contrast in features between JAS and other months, implying there is a less prominent monsoon system than the Asian monsoon.

Precipitation profiles over the Annam Range during JJAS and OND, as a function of the six candidate thermodynamic quantities, are summarized in Figs. 8 and 9, respectively. During JJAS, most of the thermodynamic parameters had consistently high correlation coefficients with PTHs, similar to the Western Ghats (Fig. 6). This suggests a similar atmospheric environment over the Annam Range and Western Ghats during JJAS, when most rain occurs (Fig. 7). In contrast, the results for OND (Fig. 9) are very different from those for JJAS (Fig. 8). The PTHs of heavy orographic rainfall increase with RH_{low} and RH_{mid}. In particular, a high positive correlation coefficient between PTH and RH_{low} was found, demonstrating that convection depth is not simply a function of humidity. It should be noted that PTHs range mostly from moderate to high during JJAS (Fig. 8), while they range from shallow to moderate during OND (Fig. 9). Although PTHs have increasing tendency with RH_{low} during OND, PTHs are still below 10 km at the highest RH_{low}. Almost no correlation with static stability of the midtroposphere (dT_v/dz_{mid}) was found during OND. Only static stability of the lowtroposphere (dT_v/dz_{low}) showed a consistently high negative correlation with PTH during both JJAS and OND. Note that the values of dT_v/dz_{low} in abscissa during OND (Fig. 9) are higher than those during JJAS (Fig. 8); thus, the ranges of PTHs during OND are lower than those during JJAS.

Yokoi and Matsumoto (2008) showed that the coexistence of a cold surge (CS) and a tropical depression-type disturbance (TDD) is important for the occurrence of heavy orographic rainfall over the Annam Range during the transition from boreal summer to winter

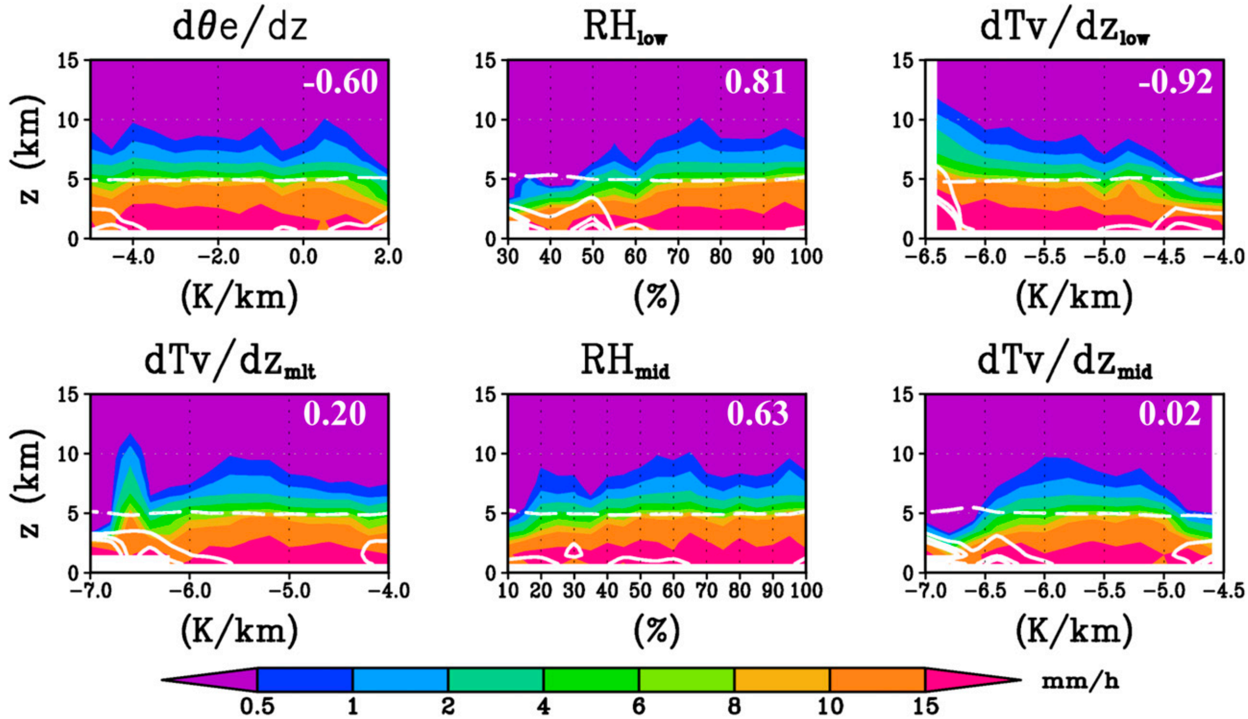

FIG. 9. As in Fig. 6, but for the Annam Range for the transition from boreal summer to winter monsoon (October–December) during the study period 2004–08.

monsoon. It is likely that heavy orographic rainfall with low PTHs occurs when a CS dominates a TDD because its northeasterly winds bring cold air, producing stronger low-level static stability, as well as surface moisture fluxes. Heavy orographic rainfall with high PTHs occurs when a TDD dominates a CS because its southerly winds supply warm and humid tropical air, weakening low-level static stability.

The static stability of the lower troposphere consistently has high absolute correlation coefficients (>0.6) with PTHs for all mountain ranges in the Asian monsoon region (Fig. 5), as well as Mexico, where strong cold-rain processes dominate and the orographic–nonorographic rainfall classification scheme was switched off in the GSMaP MWR algorithm (Yamamoto and Shige 2015). It is deemed the most important candidate determining PTHs for orographic rainfall. Low-level static stability likely inhibits cloud growth and promotes cloud detrainment.

Two-dimensional histograms of grids with heavy rainfall rates ($10 < R \leq 40\,\mathrm{mm\,h^{-1}}$) as a function of w_{oro} and dT_v/dz_{low} for the seven study areas are illustrated in Fig. 10. Results for all seasons (Fig. 10, top) for the Western Ghats and Arakan Yoma of the Indian summer monsoon region (Wang and LinHo 2002) show a clear horizontal and vertical feature at high dT_v/dz_{low} and $w_{\mathrm{oro}} = 0.02\,\mathrm{m\,s^{-1}}$. The horizontal feature mainly occurs in the summer monsoon (JJAS; Fig. 10, middle), while the vertical one is dominant in the premonsoon season (MAM; Fig. 10, bottom). These features are very similar to those shown in Fig. 7. For the Bilauktaung, Cardamom, and the Annam Range, belonging to the "buffer" zone between the Indian summer monsoon region and western North Pacific summer monsoon regions, the number of grids with heavy rain rates at low dT_v/dz_{low} is small. This is best developed for the Philippines in the western North Pacific summer monsoon region, where continental setting is less significant to the rainfall regime. Here, dT_v/dz_{low} is a better indicator of continental influence than $\mathrm{RH_{mid}}$.

Results for all seasons from Mexico also show a clear horizontal and vertical feature at high dT_v/dz_{low} and $w_{\mathrm{oro}} = 0.02\,\mathrm{m\,s^{-1}}$, as for the Western Ghats and Arakan Yoma. In Fig. 10, however, all panels for Mexico look quite similar and there are no distinct differences between the monsoon (JAS) and other seasons. This explains why the orographic–nonorographic rainfall classification scheme has low verification scores over the Sierra Madre, when it is switched on [Fig. 6d of Yamamoto and Shige (2015)].

6. Discussion

To explore PTHs in more detail, Fig. 11 shows four cases from the Western Ghats and the east coast of the

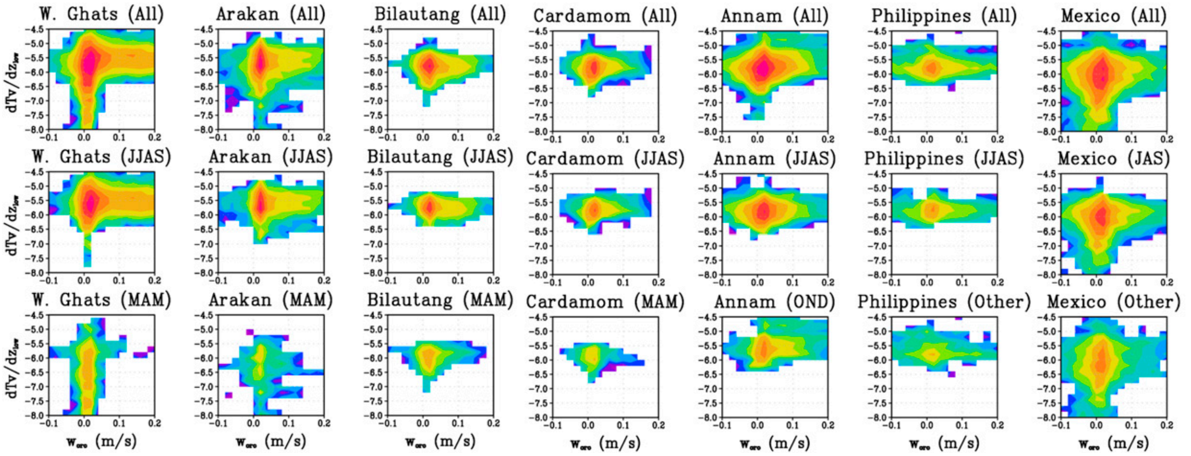

FIG. 10. As in Fig. 7, but as a function of w_{oro} and dT_v/dz_{low}.

Annam Range. Cases 1 and 2 over the Western Ghats have extreme heavy rainfalls of 70 and 110 mm h^{-1} but have marked differences in their precipitation profiles. In case 1, heavy rainfall is associated with a well-developed mesoscale convective system, consisting of deep convection with a PTH reaching 15 km, yielding stratiform precipitation. Precipitation rates above 5 mm h^{-1}, corresponding to 30.5 dBZ above the −15°C level and 31.7 dBZ at heights 750 m above the 0°C level for convective rain, reach well above the melting level (about 10 km) and manifest as active cold-rain processes (Zipser 1994; Petersen et al. 1996). In case 2, strong upward motion was orographically forced by strong westerly winds associated with Cyclone Yemyin, resulting in very heavy rainfall (above 110 mm h^{-1}) associated with a PTH lower than 10 km. The features of the precipitation profiles in case 2 are similar to those found for heavy orographic rainfall associated with Typhoon Namtheun in Japan, documented by Kubota et al. (2009, their Fig. 16). Precipitation rates above 5 mm h^{-1} were confined to within 1 km above the melting level, indicating that warm-rain processes in the lower atmosphere induce heavy rainfall.

Cases 3 and 4 for the east coast of the Annam Range are weaker than cases 1 and 2 over the Western Ghats but still have heavy rainfalls of 13 and 18 mm h^{-1}. In case

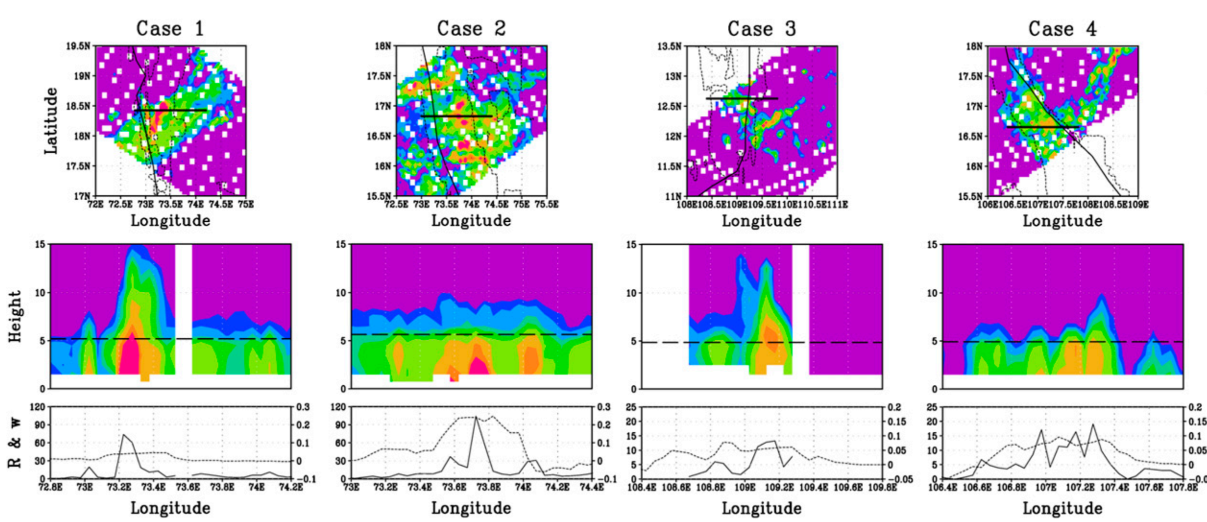

FIG. 11. Examples of cold-type and warm-type orographic rainfall over the Western Ghats (cases 1 and 2) and the Annam Range (cases 3 and 4) with corresponding TRMM orbit numbers: 48 644, 54 714, 57 017, and 56 758. (top) TRMM PR near-surface rain data and w_{oro} are represented by plan views. The black line indicates the location of the vertical cross section from (middle) TRMM PR and (bottom) their corresponding TRMM PR near-surface rain and w_{oro}. Lines indicate TRMM PR near-surface rain (scales on left y axis; mm h^{-1}) and dashed lines indicate w_{oro} (scales on right y axis; m s^{-1}).

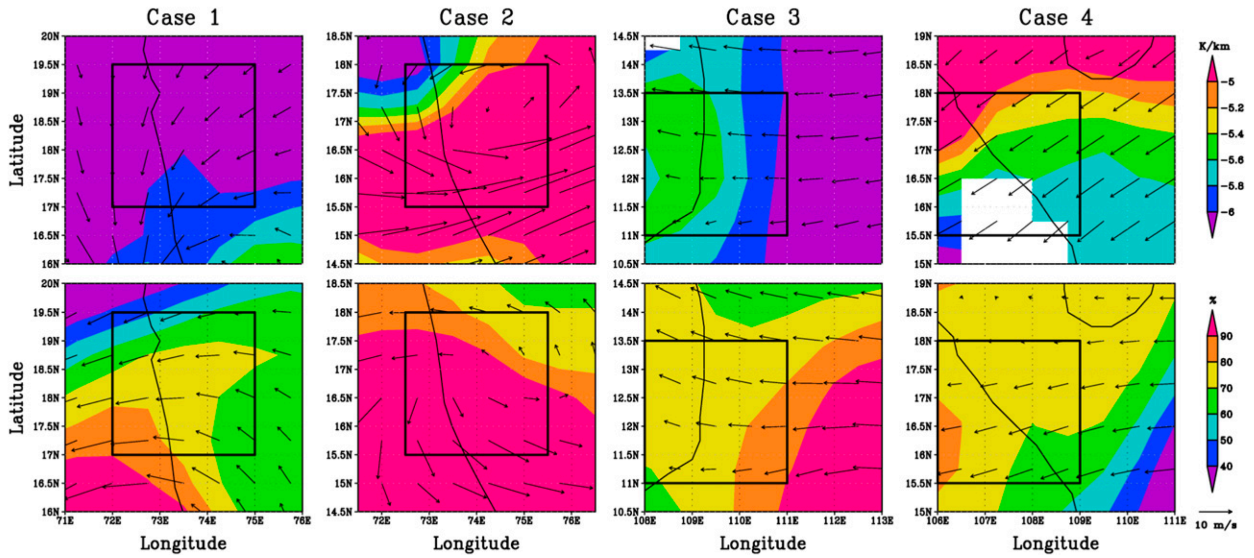

FIG. 12. Distributions of (top) dT_v/dz_{low} and $\mathbf{V}_{low}$ and (bottom) RH_{mid} and $\mathbf{V}_{mid}$ for case 1 (1800 UTC 29 May 2006), case 2 (0600 UTC 23 Jun 2007), case 3 (0000 UTC 18 Nov 2007), and case 4 (1200 UTC 1 Nov 2007). The black box indicates the location of the plan view shown in top panels of Fig. 11 for cases 1–4.

3, heavy rainfall is associated with deep convection, where PTHs and precipitation rates above 5 mm h^{-1} occur at about 13 and 10 km, respectively. This case has maximum rainfall rates at 5 km, consistent with the midlatitude and tropical continental profiles with a maximum reflectivity above the surface shown in Zipser and Lutz (1994). In contrast, case 4 had heavy rainfall associated with precipitation profiles with a PTH lower than 10 km. As in case 2, precipitation rates above 5 mm h^{-1} were confined to within 1 km above the melting level, indicating that heavy rainfall was largely induced by warm-rain processes in the lower layers of the atmosphere.

Cases 2 and 4 correspond to the warm type of Sohn et al. (2013), while cases 1 and 3 correspond to their "cold type." Figure 12 shows that the static stability of the lower troposphere (dT_v/dz_{low}) in upstream regions of cases 2 and 4 is stronger than in cases 1 and 3, consistent with results above. For the same rain class, rain areas of warm-type rain (cases 2 and 4) tend to be wider than those of the cold-type rain (cases 1 and 3). Song and Sohn (2015) showed that warm-type rain over the Korean peninsula tends to be longer lived because of the slow movement of its wider cloud system, in contrast to shorter-lived cold-type rain. The long-lived wider cloud system is thought to produce a broad region of strong static stability, leading to warm-type rain. This is clearly true for case 2, where a broad region of strong static stability resulting from the latent heat release associated with convective activities of Cyclone Yemyin was found. Stationary characteristics of orographic rainfall may also stabilize their atmospheric environments.

Meanwhile, the humidity of the midtroposphere (RH_{mid}) in upstream regions of case 2 is higher than in case 1, but RH_{mid} in upstream regions of case 4 is lower than for case 3 (Fig. 12). Humidity is unquestionably important for convection, but our study of orographic rainfall in the Asian monsoon region demonstrates that convection depth is not simply a function of humidity. During the summer monsoon, convective depth decreases with humidity, consistent with observations in Sohn et al. (2013). During the transition from boreal summer to winter monsoon, however, convective depth increases with humidity. Because these thermodynamic parameters are all influenced by large-scale circulation, it is difficult to isolate individual parameters affecting the convective depth. Using the Annam Range, we demonstrated that static stability of the lower troposphere more likely determines convection depth than humidity. This is consistent with the results of Kato et al. (2007); they showed that relatively stable atmospheric conditions produce a level of neutral buoyancy at midlevel tops (~700 hPa) that suppresses the development of deep convection over the Japanese Baiu frontal zone in June.

The differences in our results to previous studies of oceanic convection might arise from differences in the nature of the convection (ocean vs land). Takayabu (2006) found a good correlation between rain yields per flash and the tall convective rain over land, but a weaker correlation was found over the oceans. Deep convection over land is fundamentally associated with intense updrafts that are able to sustain vigorous lightning activity, while deep convection over oceans is rarely associated with such intense updrafts. It should be noted that Takayabu et al. (2010) showed that convective heating is significantly suppressed at the height of the stable layer accompanying large-scale subsidence (see their Fig. 8); they argued that entrainment of middle- to lower-tropospheric dry air is the major factor suppressing deep convection. Given that these environmental parameters are closely coupled to large-scale circulation, it is very difficult to establish the decisive factor.

In this study, we considered rainfall enhanced by orographically forced vertical motion on the windward slopes, corresponding to the stable and unstable upslope mechanisms described in Roe (2005, their Figs. 6a and 6f), Lin (2007, their Figs. 11.12a and 11.12b), and Houze (2012, their Figs. 3a and 3b). While stable upslope mechanisms have been examined by Jiang and Smith (2003), Smith (2003), Smith and Barstad (2004), and Barstad and Smith (2005) with an emphasis on mountain ranges in midlatitudes, fundamental questions about their precipitation process (warm-rain vs cold-rain processes) have not been examined. We speculate that heavy orographic rainfalls with high PTHs (cases 1 and 3) correspond to unstable upslope mechanisms, where cold-rain processes are enhanced. Those with low PTHs (cases 2 and 4) correspond to stable upslope mechanisms, where warm-rain processes are enhanced.

In the current version of the GSMaP MWR algorithm, the orographic–nonorographic rainfall classification scheme is switched on or off depending on the trimonthly database for the dominant precipitation type in $2.5° \times 2.5°$ grid boxes [Fig. 10 of Yamamoto and Shige (2015)]. As shown in Fig. 10, there are large differences in static stability between the premonsoon and the monsoon for the Indian summer monsoon region (Western Ghats and Arakan Yoma). Therefore, only using the trimonthly database, the GSMaP MWR algorithm successfully switches the orographic–nonorographic rainfall classification scheme on or off for the monsoon and the premonsoon, respectively. However, a trimonthly database for the dominant precipitation types is not sufficient for Mexico, where there are only small differences in static stability between the monsoon and other seasons. Thus, we suggest that static stability together with the orographically forced vertical motion should be derived from 6-hourly data and used for the orographic–nonorographic rainfall classification schemes not only for mountain regions in Mexico, but also to yield improvements in mountains of the Asian region.

7. Conclusions

MWR rainfall algorithms, which implicitly assume that deeper clouds with more precipitation-sized ice are more likely to produce heavy rainfall, are known to underestimate rainfall over coastal mountain ranges during the moist Asian monsoon, when heavy rainfall is frequently associated with low PTHs. Problems identified in the MWR rainfall algorithms have led to fundamental questions about what thermodynamic parameters determine PTHs. We examined relationships between six thermodynamic characteristics of the atmosphere and the PTHs of relatively heavy orographic rainfall in coastal mountains in the tropics to explore this issue.

Most of these parameters had high correlation coefficients with PTHs in western Asian mountain regions (Western Ghats, Arakan Yoma, Bilauktaung, and Cardamom) and Mexico. It was difficult to identify the key parameter determining the PTHs in these regions, since most of these thermodynamic parameters are influenced by large-scale circulation. Instead, we focused our study on the Annam Range, where there is a broad range of environmental conditions because of onshore northeasterly monsoon winds from the South China Sea, as well as on the Western Ghats, where shallow orographic rainfall appears frequently.

Static stability near the 0°C level (dT_v/dz_{mlt}) had low absolute correlation coefficients, especially over the Western Ghats, where other thermodynamic parameters had high correlation coefficients, reflecting shallow convection with relatively little stratiform precipitation. These results are consistent with previous studies of tropical oceanic convection (Takemi et al. 2004; Jensen and DelGenio 2006; Takayabu et al. 2006, 2010) that showed that static stability near the 0°C level is not effective at limiting oceanic congestus cloud-top heights. However, the PTHs of heavy orographic rainfall generally decreased with low-level and midlevel increases in relative humidity, differing from previous studies that showed that a drying of the midtroposphere effectively limits oceanic congestus cloud-top heights. In fact, the PTHs over the Annam Range increased with low-level and midlevel increases in relative humidity during the transition from boreal summer to winter monsoon, demonstrating that convection depth is not simply a function of humidity.

The PTHs of heavy orographic rainfall decreased with low-level stability for all regions in this study, as well as for the Annam Range during the transition from boreal summer to winter monsoon. Therefore, low-level static stability, which inhibits cloud growth and promotes cloud detrainment, is inferred to be the key parameter determining PTH. Thus, heavy orographic rainfall results from both shallow clouds associated with stable upslope mechanisms, as well as deep clouds associated with unstable upslope mechanisms.

Our results are only for heavy orographic rainfall on windward slopes of coastal mountains ranges in the tropics. Recently, Hamada et al. (2015) showed that most extreme rainfall events in the tropics and subtropics are characterized by less intense convection with intense radar echoes that do not extend to extremely high altitudes. This implies that warm-rain processes are crucial to producing extremely high rainfall rates. Our approach could easily be extended to explore such extreme rainfall events. We also plan to use low-level static stability to improve MWR algorithms (i.e., GPROF and GSMaP) in mountainous areas.

Acknowledgments. This study was mainly carried out during S. Shige's sabbatical visit to Colorado State University. He expresses special thanks to the late Professor Takehiko Satomura for allowing him to take a sabbatical leave. Wes Berg, Paula Brown, Dave Randel and Paul Ciesielski helped with computing, while Munehisa K. Yamamoto edited the SRTM30 data. This study is supported by JSPS KAKENHI Grants 23681037 and 26282109 and the JAXA Precipitation Measuring Mission (PMM) project. The authors thank three anonymous reviewers for their constructive comments that improved the clarity of the paper.

REFERENCES

Adams, D. K., and A. C. Comrie, 1997: The North American monsoon. *Bull. Amer. Meteor. Soc.*, **78**, 2197–2213, doi:10.1175/1520-0477(1997)078<2197:TNAM>2.0.CO;2.

Aonashi, K., and Coauthors, 2009: GSMaP passive microwave precipitation retrieval algorithm: Algorithm description and validation. *J. Meteor. Soc. Japan*, **87A**, 119–136, doi:10.2151/jmsj.87A.119.

Barstad, I., and R. B. Smith, 2005: Evaluation of an orographic precipitation model. *J. Hydrometeor.*, **6**, 85–99, doi:10.1175/JHM-404.1.

Byers, H. R., and R. R. Braham Jr., 1949: *The Thunderstorm: Final Report of the Thunderstorm Project*. U.S. Government Printing Office, 282 pp.

Chang, C.-P., Z. Wang, J. McBride, and C.-H. Liu, 2005: Annual cycle of Southeast Asia—Maritime Continent rainfall and the asymmetric monsoon transition. *J. Climate*, **18**, 287–301, doi:10.1175/JCLI-3257.1.

Cotton, W. R., G. Bryan, and S. C. van den Heever, 2011: *Storm and Cloud Dynamics*. Academic Press, 820 pp.

Dee, D. P., and Coauthors, 2011: The ERA-Interim reanalysis: Configuration and performance of the data assimilation system. *Quart. J. Roy. Meteor. Soc.*, **137**, 553–597, doi:10.1002/qj.828.

Douglas, M. W., R. Maddox, K. Howard, and S. Reyes, 1993: The Mexican monsoon. *J. Climate*, **6**, 1665–1667, doi:10.1175/1520-0442(1993)006<1665:TMM>2.0.CO;2.

Ebert, E. E., and M. J. Manton, 1998: Performance of satellite rainfall estimation algorithms during TOGA COARE. *J. Atmos. Sci.*, **55**, 1537–1557, doi:10.1175/1520-0469(1998)055<1537:POSREA>2.0.CO;2.

Farr, T. G., and Coauthors, 2007: The Shuttle Radar Topography Mission. *Rev. Geophys.*, **45**, RG2004, doi:10.1029/2005RG000183.

Ferraro, R., and Coauthors, 2005: NOAA operational hydrological products derived from the Advanced Microwave Sounding Unit. *IEEE Trans. Geosci. Remote Sens.*, **43**, 1036–1049, doi:10.1109/TGRS.2004.843249.

Hamada, A., Y. N. Takayabu, C. Liu, and E. J. Zipser, 2015: Weak linkage between the heaviest rainfall and tallest storms. *Nat. Commun.*, **6**, 6213, doi:10.1038/ncomms7213.

Houze, R. A., Jr., 2012: Orographic effects on precipitating clouds. *Rev. Geophys.*, **50**, RG1001, doi:10.1029/2011RG000365.

——, 2014: *Cloud Dynamics*. 2nd ed. Academic Press, 432 pp.

Hoyos, C. D., and P. J. Webster, 2007: The role of intraseasonal variability in the nature of Asian monsoon precipitation. *J. Climate*, **20**, 4402–4424, doi:10.1175/JCLI4252.1.

Iguchi, T., T. Kozu, J. Kwiatkowski, R. Meneghini, J. Awaka, and K. Okamoto, 2009: Uncertainties in the rain profiling algorithm for the TRMM precipitation radar. *J. Meteor. Soc. Japan*, **87A**, 1–30, doi:10.2151/jmsj.87A.1.

Jensen, M. P., and A. D. Del Genio, 2006: Factors limiting convective cloud-top height at the ARM Nauru Island climate research facility. *J. Climate*, **19**, 2105–2117, doi:10.1175/JCLI3722.1.

Jiang, Q., and R. B. Smith, 2003: Cloud timescales and orographic precipitation. *J. Atmos. Sci.*, **60**, 1543–1559, doi:10.1175/2995.1.

Johnson, R. H., P. E. Ciesielski, and K. A. Hart, 1996: Tropical inversions near the 0°C level. *J. Atmos. Sci.*, **53**, 1838–1855, doi:10.1175/1520-0469(1996)053<1838:TINTL>2.0.CO;2.

——, T. M. Rickenbach, S. A. Rutledge, P. E. Ciesielski, and W. H. Schubert, 1999: Trimodal characteristics of tropical convection. *J. Climate*, **12**, 2397–2418, doi:10.1175/1520-0442(1999)012<2397:TCOTC>2.0.CO;2.

Kato, T., S. Hayashi, and M. Yoshizaki, 2007: Statistical study on cloud top height of cumulonimbi thermodynamically estimated from objective analysis data during the Baiu season. *J. Meteor. Soc. Japan*, **85**, 529–557, doi:10.2151/jmsj.85.529.

Kubota, T., T. Ushio, S. Shige, S. Kida, M. Kachi, and K. Okamoto, 2009: Verification of high-resolution satellite-based rainfall estimates around Japan using a gauge-calibrated ground-radar dataset. *J. Meteor. Soc. Japan*, **87A**, 203–222, doi:10.2151/jmsj.87A.203.

Kumar, S., A. Hazra, and B. N. Goswami, 2014: Role of interaction between dynamics, thermodynamics and cloud microphysics on summer monsoon precipitating clouds over the Myanmar coast and the Western Ghats. *Climate Dyn.*, **43**, 911–924, doi:10.1007/s00382-013-1909-3.

Kummerow, C., W. Barnes, T. Kozu, J. Shiue, and J. Simpson, 1998: The Tropical Rainfall Measuring Mission (TRMM) sensor package. *J. Atmos. Oceanic Technol.*, **15**, 809–817, doi:10.1175/1520-0426(1998)015<0809:TTRMMT>2.0.CO;2.

——, D. L. Randel, M. Kulie, N.-Y. Wang, R. Ferraro, S. J. Munchak, and V. Petkovic, 2015: The evolution of the Goddard profiling algorithm to a fully parametric scheme. *J. Atmos. Oceanic Technol.*, **32**, 2265–2280, doi:10.1175/JTECH-D-15-0039.1.

Kwon, E.-H., B.-J. Sohn, D.-E. Chang, M.-H. Ahn, and S. Yang, 2008: Use of numerical forecasts for improving TMI rain retrievals over the mountainous area in Korea. *J. Appl. Meteor. Climatol.*, **47**, 1995–2007, doi:10.1175/2007JAMC1857.1.

Lin, Y.-L., 2007: *Mesoscale Dynamics*. Cambridge University Press, 630 pp.

Manohar, G. K., S. S. Kandalgaonkar, and M. I. R. Tinmaker, 1999: Thunderstorm activity over India and the Indian southwest monsoon. *J. Geophys. Res.*, **104**, 4169–4188, doi:10.1029/98JD02592.

McCollum, J. R., and R. R. Ferraro, 2003: Next generation of NOAA/NESDIS TMI, SSM/I, and AMSR-E microwave land rainfall algorithms. *J. Geophys. Res.*, **108**, 8382, doi:10.1029/2001JD001512.

Murakami, T., and J. Matsumoto, 1994: Summer monsoon over the Asian continent and western North Pacific. *J. Meteor. Soc. Japan*, **72**, 719–745.

Petersen, W. A., and S. A. Rutledge, 2001: Regional variability in tropical convection: Observations from TRMM. *J. Climate*, **14**, 3566–3586, doi:10.1175/1520-0442(2001)014<3566:RVITCO>2.0.CO;2.

——, ——, and R. E. Orville, 1996: Cloud-to-ground lightning observations from TOGA COARE: Selected results and lightning location algorithms. *Mon. Wea. Rev.*, **124**, 602–620, doi:10.1175/1520-0493(1996)124<0602:CTGLOF>2.0.CO;2.

Richards, F., and P. Arkin, 1981: On the relationship between satellite observed cloud cover and precipitation. *Mon. Wea. Rev.*, **109**, 1081–1093, doi:10.1175/1520-0493(1981)109<1081:OTRBSO>2.0.CO;2.

Roe, G. H., 2005: Orographic precipitation. *Annu. Rev. Earth Planet. Sci.*, **33**, 645–671, doi:10.1146/annurev.earth.33.092203.122541.

Rotunno, R., J. B. Klemp, and M. Weisman, 1988: A theory for strong, long-lived squall lines. *J. Atmos. Sci.*, **45**, 463–458, doi:10.1175/1520-0469(1988)045<0463:ATFSLL>2.0.CO;2.

Sakakibara, H., 1981: Heavy rainfall from very shallow convective clouds. *J. Meteor. Soc. Japan*, **59**, 387–394.

Sherwood, S. C., 1999: Convective precursors and predictability in the tropical western Pacific. *Mon. Wea. Rev.*, **127**, 2977–2991, doi:10.1175/1520-0493(1999)127<2977:CPAPIT>2.0.CO;2.

Shige, S., Y. N. Takayabu, W.-K. Tao, and D. E. Johnson, 2004: Spectral retrieval of latent heating profiles from TRMM PR data. Part I: Development of a model-based algorithm. *J. Appl. Meteor.*, **43**, 1095–1113, doi:10.1175/1520-0450(2004)043<1095:SROLHP>2.0.CO;2.

——, ——, ——, and C.-L. Shie, 2007: Spectral retrieval of latent heating profiles from TRMM PR data. Part II: Algorithm improvement and heating estimates over tropical ocean regions. *J. Appl. Meteor. Climatol.*, **46**, 1098–1124, doi:10.1175/JAM2510.1.

——, ——, and ——, 2008: Spectral retrieved of latent heating profiles from TRMM PR data. Part III: Moistening estimates over the tropical ocean regions. *J. Appl. Meteor. Climatol.*, **47**, 620–640, doi:10.1175/2007JAMC1738.1.

——, and Coauthors, 2009a: The GSMaP precipitation retrieval algorithm for microwave sounders—Part I: Over-ocean algorithm. *IEEE Trans. Geosci. Remote Sens.*, **47**, 3084–3097, doi:10.1109/TGRS.2009.2019954.

——, Y. N. Takayabu, S. Kida, W.-K. Tao, X. Zeng, and T. L'Ecuyer, 2009b: Spectral retrieved of latent heating profiles from TRMM PR data. Part VI: Comparisons of lookup tables from two- and three-dimensional simulations. *J. Climate*, **22**, 5577–5594, doi:10.1175/2009JCLI2919.1.

——, S. Kida, H. Ashiwake, T. Kubota, and K. Aonashi, 2013: Improvement of TMI rain retrievals in mountainous areas. *J. Appl. Meteor. Climatol.*, **52**, 242–254, doi:10.1175/JAMC-D-12-074.1.

——, M. K. Yamamoto, and A. Taniguchi, 2015: Improvement of TMI rain retrieval over the Indian subcontinent. *Remote Sensing of the Terrestrial Water Cycle*, *Geophys. Monogr.*, Vol. 206, Amer. Geophys. Union, 27–42, doi:10.1002/9781118872086.ch2.

Smith, R. B., 2003: A linear upslope-time-delay model for orographic precipitation. *J. Hydrol.*, **282**, 2–9, doi:10.1016/S0022-1694(03)00248-8.

——, and I. Barstad, 2004: A linear theory of orographic precipitation. *J. Atmos. Sci.*, **61**, 1377–1391, doi:10.1175/1520-0469(2004)061<1377:ALTOOP>2.0.CO;2.

Sohn, B. J., G.-H. Ryu, H.-J. Song, and M.-L. Ou, 2013: Characteristic features of warm-type rain producing heavy rainfall over the Korean peninsula inferred from TRMM measurements. *Mon. Wea. Rev.*, **141**, 3873–3888, doi:10.1175/MWR-D-13-00075.1.

Song, H.-J., and B.-J. Sohn, 2015: Two heavy rainfall types over the Korean peninsula in the humid East Asian summer environment: A satellite observation study. *Mon. Wea. Rev.*, **143**, 363–382, doi:10.1175/MWR-D-14-00184.1.

Spencer, R. W., 1984: Satellite passive microwave rain rate measurement over croplands during spring, summer and fall. *J. Climate Appl. Meteor.*, **23**, 1553–1562, doi:10.1175/1520-0450(1984)023<1553:SPMRRM>2.0.CO;2.

Stensrud, D. J., 1996: Importance of low-level jets to climate: A review. *J. Climate*, **9**, 1698–1711, doi:10.1175/1520-0442(1996)009<1698:IOLLJT>2.0.CO;2.

Takayabu, Y. N., 2006: Rain-yield per flash calculated from TRMM PR and LIS data and its relationship to the contribution of tall convective rain. *Geophys. Res. Lett.*, **33**, L18705, doi:10.1029/2006GL027531.

——, J. Yokomori, and K. Yoneyama, 2006: A diagnostic study on interactions between atmospheric thermodynamic structure and cumulus convection over the tropical western Pacific Ocean and over the Indochina Peninsula. *J. Meteor. Soc. Japan*, **84A**, 151–169, doi:10.2151/jmsj.84A.151.

——, S. Shige, W.-K. Tao, and N. Hirota, 2010: Shallow and deep latent heating modes over tropical oceans observed with TRMM PR spectral latent heating data. *J. Climate*, **23**, 2030–2046, doi:10.1175/2009JCLI3110.1.

Takeda, T., and K. Takase, 1980: Radar observation of rainfall system modified by orographic effects. *J. Meteor. Soc. Japan*, **58**, 500–516.

——, N. Moriyama, and Y. Iwasaka, 1976: A case study of heavy rain in Owase area. *J. Meteor. Soc. Japan*, **54**, 32–41.

Takemi, T., O. Hirayama, and C. Liu, 2004: Factors responsible for the vertical development of tropical oceanic cumulus convection. *Geophys. Res. Lett.*, **31**, L11109, doi:10.1029/2004GL020225.

Taniguchi, A., and Coauthors, 2013: Improvement of high-resolution satellite rainfall product for Typhoon Morakot (2009) over Taiwan. *J. Hydrometeor.*, **14**, 1859–1871, doi:10.1175/JHM-D-13-047.1.

Tao, W.-K., S. Lang, X. Zeng, S. Shige, and Y. Takayabu, 2010: Relating convective and stratiform rain to latent heating. *J. Climate*, **23**, 1874–1893, doi:10.1175/2009JCLI3278.1.

Wang, B., and LinHo, 2002: Rainy seasons of the Asian–Pacific monsoon. *J. Climate*, **15**, 386–398, doi:10.1175/1520-0442(2002)015<0386:RSOTAP>2.0.CO;2.

Weng, F., L. Zhao, R. R. Ferraro, G. Poe, X. Li, and N. C. Grody, 2003: Advanced microwave sounding unit cloud and precipitation algorithms. *Radio Sci.*, **38**, 8068, doi:10.1029/2002RS002679.

Werner, M., 2001: Shuttle Radar Topography Mission (SRTM) mission overview. *Frequenz*, **55**, 75–79, doi:10.1515/FREQ.2001.55.3-4.75.

Xie, S. P., H. M. Xu, N. H. Saji, Y. Q. Wang, and W. T. Liu, 2006: Role of narrow mountains in large-scale organization of Asian monsoon convection. *J. Climate*, **19**, 3420–3429, doi:10.1175/JCLI3777.1.

Yamamoto, M. K., and S. Shige, 2015: Implementation of an orographic/nonorographic rainfall classification scheme in the GSMaP algorithm for microwave radiometers. *Atmos. Res.*, **163**, 36–47, doi:10.1016/j.atmosres.2014.07.024.

Yanai, M., S. Esbensen, and J.-H. Chu, 1973: Determination of bulk properties of tropical cloud clusters from large-scale heat and moisture budgets. *J. Atmos. Sci.*, **30**, 611–627, doi:10.1175/1520-0469(1973)030<0611:DOBPOT>2.0.CO;2.

Yasunaga, K., and Coauthors, 2006: Melting layer cloud observed during R/V *Mirai* cruise MR01-K05. *J. Atmos. Sci.*, **63**, 3020–3032, doi:10.1175/JAS3779.1.

Yokoi, S., and J. Matsumoto, 2008: Collaborative effects of cold surge and tropical depression–type disturbance on heavy rainfall in central Vietnam. *Mon. Wea. Rev.*, **136**, 3275–3287, doi:10.1175/2008MWR2456.1.

Zhang, C. Z., H. Uyeda, H. Yamada, B. Geng, and Y. Ni, 2006: Characteristics of mesoscale convective systems over east part of continental China during the Meiyu from 2001 to 2003. *J. Meteor. Soc. Japan*, **84**, 763–782, doi:10.2151/jmsj.84.763.

Zipser, E. J., 1994: Deep cumulonimbus cloud systems in the Tropics with and without lightning. *Mon. Wea. Rev.*, **122**, 1837–1851, doi:10.1175/1520-0493(1994)122<1837:DCCSIT>2.0.CO;2.

——, and K. R. Lutz, 1994: The vertical profile of radar reflectivity of convective cells: A strong indicator of storm intensity and lightning probability? *Mon. Wea. Rev.*, **122**, 1751–1759, doi:10.1175/1520-0493(1994)122<1751:TVPORR>2.0.CO;2.